



RESEARCH ARTICLE

Very high V_{OC} and FF of CdTe thin-film solar cells with the applications of organo-metallic halide perovskite thin film as a hole transport layer

Khagendra P. Bhandari¹ | Fadhil K. Alfadhili² | Ebin Bastola² |
Suneth C. Watthage² | Zhaoning Song² | Geethika K. Liyanage² |
Adam J. Phillips² | Michael J. Heben² | Randy J. Ellingson²

¹Department of Physics and Astronomy, Ohio Northern University, 525 South Main Street, Ada, OH, 45810, USA

²Wright Center for Photovoltaics Innovation and Commercialization, Department of Physics and Astronomy, University of Toledo, 2801 W. Bancroft Street, Toledo, OH, 43606, USA

Correspondence

Khagendra Bhandari, Department of Physics and Astronomy, Ohio Northern University, 525 S Main Street, Ada, OH 45810, USA.
Email: k-bhandari@onu.edu

Funding information

Air Force Research Laboratory, Grant/Award Number: FA9453-11-C-0253; National Science Foundation, Grant/Award Number: CHE-1230246

Abstract

We fabricate and characterize methylammonium lead halide perovskite film as a novel back contact to CdTe thin-film solar cells. We apply $\sim 0.75 \mu\text{m}$ perovskite film at the interface of CdCl_2 -activated and Cu-doped CdTe surface and complete the device with Au back contact. We use Cu/Au back contact as a reference to compare results with novel back contact. Our investigation shows that incorporation of thin layer of perovskite film before the back contact metal reduces back contact barrier effect and improves fill factor (FF) and open-circuit voltage (V_{OC}) of the solar cells. Our low temperature JV results prove that thin-film perovskite is a very necessary component in CdTe solar cells to reduce back contact barrier, to minimize interface or surface recombination, to improve collection efficiencies, and to increase the efficiency of solar cells. Our best device shows 7% increase in V_{OC} to 0.875 V and $\sim 7\%$ increase in FF with the highest FF of 81%, and solar cell's efficiency finally increases by 10% with the use of $\text{MAPb}(\text{I}_{1-x}\text{Br}_x)_3$ as an interface layer.

KEYWORDS

back contact, cadmium telluride, fill factor, halide perovskite, hole transport, open-circuit voltage, thin film

1 | INTRODUCTION

With a bandgap of 1.45 eV and high absorption coefficient ($>10^4 \text{ cm}^{-1}$) near the band edge, CdTe is an excellent material for photovoltaic technology.¹ However, the laboratory-scale best CdTe solar cell's efficiency is still $\sim 25\%$ less than that of its detailed balance limit.^{2,3} The back contact on CdTe thin-film solar cells has great importance for both scientific and industrial interests as it influences the efficiency and long-term stability of the solar cells. The development of an efficient back contact on p-CdTe is a difficult task because of high electron affinity and bandgap of CdTe. As the work function of commonly available metals is smaller than the work function of CdTe, Schottky junction is formed at the CdTe/back contact metal

interface.⁴ The diode formed at the CdTe/metal interface has direction opposite to the p-n junction diode formed at CdS/CdTe hetero-interface and lowers the overall built-in potential and open-circuit voltage (V_{OC}) of the solar cells. The CdTe solar cell's efficiency is mostly affected by excessive nonradiative recombination loss due to the high contact resistance and the difficulty in increasing the acceptor concentration by p-type doping.⁵ The most common practice of reducing the back contact barrier is to increase the p-type carrier concentration of CdTe by using elemental Cu diffusion, which narrows depletion width at CdTe/Au interface and may create pseudo-ohmic contact so that the photogenerated holes tunnel through the barrier to reach back contact metal.⁶ With this method, however, barrier-free interface is not expected, and full benefit in performance is not

achieved.^{7,8} It is also known that Cu doping alone, without an additional layer, has had limitations. Commonly used Cu containing back contact materials for CdTe solar cells are Cu/graphite,⁹ ZnTe:Cu,^{10,11} Cu/FeS₂,^{12,13} and graphite paste doped with HgTe and CuTe.¹⁴ Among these back contacts, ZnTe:Cu plays an important role in device performance as the First Solar reaches efficiency of higher than 22% with its application.¹⁵ It is believed that using ZnTe as an interlayer improves the valence band offset to p-type CdTe because of its wide bandgap of 2.26 eV and with its optimized work function establishes a more ohmic and stable back contact.^{10,16} In the environmental point of view, ZnTe is considered safe as it does not contain heavy metals, but it contains the rare earth element Te and its deposition technique is not cost effective. Also, from the theoretical point of view, ZnTe/CdTe heterojunction is not highly desirable because of the mismatch of their lattice constants.¹⁷ The replacement of ZnTe may be necessary to alleviate these problems. Similarly, Bhandari et al. demonstrated some improvement in V_{OC} and fill factor (FF) of CdTe solar cells with the application of Cu/FeS₂/Au back contacts,^{12,13} but lots of rooms, still available for the improvement, cannot be fulfilled by these back contacts.

The highest V_{OC} for thin-film CdTe solar cells is only about 72% of its detailed balance limit, which is the indication of significant voltage deficit.¹⁸ This voltage limitation is primarily due to the low carrier densities and low recombination lifetimes of the material. One of the prerequisites for high V_{OC} in CdTe solar cells is to achieve a high quasi-Fermi level splitting determined by long bulk carrier lifetime and low interface recombination velocity.¹⁹ However, low carrier lifetime and low achievable doping levels limit quasi-Fermi level splitting in polycrystalline CdTe solar cells. The effective built-in voltage inside the CdTe solar cells is smaller than the achievable quasi-Fermi level splitting in the absorber layer, and this situation decreases the V_{OC} of the solar cells. Therefore, keeping the doping concentration in CdTe constant, a suitable hole transport layer has been a subject of interest to minimize the back barrier effects, to reduce back contact interface recombination velocity, and to enhance device performance. In this work, we have developed organo-metallic halide perovskite (methylammonium lead halide, CH₃NH₃Pb(I_{1-x}Br_x)₃ or MAPb(I_{1-x}Br_x)₃) thin film as a hole transport layer for CdS/CdTe solar cells and have achieved tremendous success in the device performances with record to high V_{OC} and FF for CdS/CdTe heterojunction.

The organo-metallic halide perovskites possess several outstanding optoelectronic properties that make them ideal for photovoltaic (PV) application.²⁰⁻²³ As a result of the tremendous research efforts across the world, perovskite-based solar cells are now comparable with other previously existing highly efficient technologies at least in the lab scale.²⁴⁻²⁶ Unlike ZnTe, MAPb(I_{1-x}Br_x)₃ thin films are easily synthesized in solution-based method and easily deposited at low annealing temperature. Because the ZnTe contact layer must be deposited onto finished CdS/CdTe PV device structures, deposition processes that use high deposition temperatures ($\geq 300^\circ\text{C}$) is expected to include impurity diffusion through grain boundaries in the CdTe.²⁷ For high-quality crystalline p⁺-ZnTe, high temperature route such as molecular beam epitaxy is preferred.²⁸ The perovskite material is

easily available, and heavy metal Pb can be substituted by environmentally friendly elements such as Sn or Ge. In this work, we have demonstrated the application of MAPb(I_{1-x}Br_x)₃ film as an interface layer or back contact layer to CdTe thin-film solar cell. This work is the updated and optimization version of our previous work wherein the efficiency has been increased by >8.0%.²⁹ Our initial results are very promising with very high V_{OC} of 0.875 V and very high FF of 81% from a single-junction CdTe thin-film solar cells. Another important benefit of using perovskite as an interface layer with CdTe is because of lattice matching in CdTe/MAPb(I_{1-x}Br_x)₃ heterojunction.³⁰

2 | EXPERIMENTAL DETAILS

2.1 | Methylammonium lead halide perovskite thin-film fabrication

Single-step deposition method was used to fabricate MAPb(I_{1-x}Br_x)₃ films on glass and CdTe substrates with a method described elsewhere.³¹ Precursor solutions for the perovskite fabrication were made by dissolving different concentration of lead (II) iodide (PbI₂), methylammonium iodide (MAI), lead (II) bromide (PbBr₂), and methylammonium bromide (MABr) in a mixed solution of anhydrous dimethylformamide (DMF) and dimethyl sulfoxide (DMSO) (4:1, volume ratio). The molar concentration of PbI₂ and MAI were decreased from 0.9 to 0.1 in the interval of 0.2 when the molar concentration of PbBr₂ and MABr were increased from 0.1 to 0.9 in the same interval to vary iodine (I) and bromine (Br) concentration in the solution. The precursor solution so obtained was spin-coated on the CdTe thin-film substrate at 1000 rpm for 10 s and 4,000 rpm for 25 s at room temperature ($\sim 20^\circ\text{C}$). For the improvement in performance, substrate temperature was made slightly smaller than the room temperature ($\sim 15^\circ\text{C}$) during the deposition of perovskite film. During the second step, $\sim 550 \mu\text{l}$ of anhydrous ethyl ether or anhydrous ethyl acetate was dropped on the spinning sample ~ 17 s prior to the end. Then, the samples were annealed at 110°C hotplate temperature for 30 min to form MAPb(I_{1-x}Br_x)₃. The value of x is varied from 0.1 to 0.9.

2.2 | Solar cells fabrications

Sputtered deposition method was used to deposit thin layer of cadmium sulfide (CdS), and vapor transport deposition (VTD) mechanism was applied to fabricate cadmium telluride (CdTe), an absorber layer in CdS/CdTe thin-film solar cells. In VTD process, saturated vapor of Cd and Te (S) species is prepared and is delivered to the CdS layer deposited onto TEC™ 15 soda lime glass substrates coated with a 100-nm thick high-resistivity transparent layer (HR; Pilkington N. A.) at low temperature where the vapor becomes less saturated resulting in CdTe film formation.³² About 3 nm Cu was deposited onto CdCl₂-treated CdTe and annealed in dry air at 150°C for 20 min. A thin layer of MAPb(I_{1-x}Br_x)₃ of thickness ~ 750 nm was then deposited onto doped CdTe using a spin coating and further annealing the device at 110°C for 30 min. Finally, the device was completed by depositing

~40 nm Au on top of MAPb(I_{1-x}Br_x)₃. For the comparison, reference devices were prepared with a standard (Cu/Au) back contacts, where deposition of Cu and Au was made identically with that of another back contact.

2.3 | Current density-voltage (J-V) measurement

Current density-voltage (JV) measurement was recorded using a Keithley 2440 source meter and a solar simulator (Newport model 91195A-1000). Solar simulator was calibrated to configure the light intensity of 100 mW/cm² equivalent to AM1.5G using a standard Si photodiode. The cell area (~0.08 cm²) is defined by laser scribing.

2.4 | EQE measurement

External quantum efficiency (EQE) measurement was conducted to confirm J_{SC} values obtained from J-V measurement. The EQE spectra were obtained in the spectral range of 300 to 910 nm from a source (PV Measurements, Inc. with a model # IVQE8-C) having similar light source as that of J-V system.

2.5 | Schottky barrier height calculation (Φ_b)

Temperature-dependent current voltage characteristics were performed to calculate barrier height developed at the back contact interface. Current voltage data were collected in the temperature range of 180 K to 300 K using a system of helium cryostat for both dark and light measurements.

2.6 | Other characterization methods

A field emission scanning electron microscope (Hitachi S-4800) was used to acquire scanning electron microscopy (SEM) images of CdTe surfaces and device cross sections. The X-ray diffraction (XRD) pattern of the perovskite films were taken using a RigakuUltima III X-ray diffractometer fitted with small angle X-ray scattering (SAXS) at 40 kV accelerating voltage and 44 mA current. Unpolarized transmittance and reflectance spectra of the films were taken using a PerkinElmer Lambda 1050 UV/VIS/NIR spectrophotometer.

3 | RESULTS AND DISCUSSIONS

As an interface layer in back contact, MAPb(I_{1-x}Br_x)₃ films were prepared on Cu-doped CdTeas substrates. Before directly applying them on devices, characterization of the films was first completed by fabricating them on soda lime glass substrates. Figure 1A shows absorbance spectra of perovskite films with different Br concentrations. It is found that as Br concentration increases, the absorbance

edges shift to shorter wavelength values, indicating the increase of the bandgap energies. The bandgap (estimated from the onset absorbance band using Tauc plot) variation with the Br content in MAPb(I_{1-x}Br_x)₃ is plotted in Figure S1. This finding is consistent with works of Noh et al. and Sadhanala et al., who demonstrated perovskite bandgap tuning by varying the halide composition (Br/I) in the perovskite precursor solution.^{33,34} Mosconi et al. describes the increase of bandgap energy as the structural distortion caused by the change in stress of Pb-I bonds after Br inclusion.³⁵

Figure 1B shows the XRD patterns monitored in the 2θ range of 10°–50° for MAPb(I_{1-x}Br_x)₃ varying x from 0 to 1. As shown in the figure, as the Br concentration is increased, the diffraction peaks are shifted toward higher diffraction angles and matches very well with the previous reports.^{33,36,37} The shift of diffraction angles is caused by decrease of lattice spacing due to the partial substitution of the larger (ionic radius of iodine 2.2 Å) iodine atom with a smaller (ionic radius of bromine 1.96 Å) bromine atom. The diffraction profile in Figure 1B belongs to cubic perovskite with a space group of Pm3m and is in good agreement with previous reports in the literature.³⁶ On the basis of the existence of only two peaks of cubic crystal structures for MAPbI₃, peaks corresponding to their tetragonal phases have been

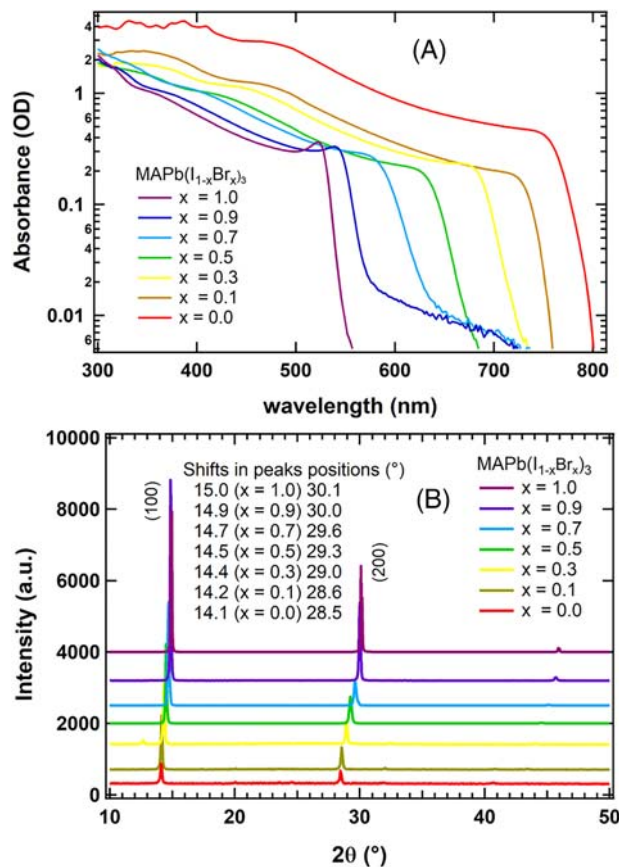


FIGURE 1 A, UV-vis absorption spectra of MAPb(I_{1-x}Br_x)₃ films measured using an integral sphere. B, X-ray diffractograms of MAPb(I_{1-x}Br_x)₃ (x = 0, 0.2, 0.4, 0.6, 0.8, 1.0) perovskite thin films [Colour figure can be viewed at wileyonlinelibrary.com]

missing. In a similar study, Noh et al. found linear relationship of lattice parameters with Br concentration.³³ With these two characterizations, we confirmed that $\text{MAPb}(\text{I}_{1-x}\text{Br}_x)_3$ films were pure without any traces of impurities.

In XRD patterns, the peak position is related to the lattice constant of the material. The lattice constant of cubic CdTe thin-film grown on glass/ SnO_2 substrate by close space sublimation (CSS) method is 6.48 Å.³⁸ Similarly, lattice constants of MAPbI_3 and MAPbBr_3 in their cubic crystal structures are 6.4 and 5.9 Å, respectively.³⁹ When we calculated lattice constants of mixed perovskite considering peak at $2\theta \sim 15^\circ$ in Figure 1B, we found them as 5.90, 5.94, 6.02, 6.10, 6.15, and 6.30 Å, respectively, for $x = 1, 0.9, 0.7, 0.5, 0.3, 0.1$, and 0.0. From this, we learn that lattice constants of perovskite are slightly deviated from CdTe when the Br concentration is increased. With this, we started their new application as an interface layer or hole transport layer in back contact of CdTe thin-film solar cells.

Device structure of CdS/CdTe solar cells with novel back contact is shown in Figure 2 along with its SEM cross-sectional imaging. The cross-sectional imaging shows very clear layers of front contact, window layer, absorber layer, and some of the back contacts. The 3-nm Cu diffuses into CdTe after annealing the device, and 40-nm Au layer is on top of perovskite layer. In the device structure, carriers are mainly generated in CdTe absorber layer and are separated by the built-in electric field at CdS/CdTe interface. Electrons are then transferred from the conduction band of CdTe to CdS, and ultimately, they are collected at the front electrode. The photogenerated holes from the valence band of CdTe are moved to the $\text{MAPb}(\text{I}_{1-x}\text{Br}_x)_3$ interface layer and are collected by the Au electrode. The $\text{MAPb}(\text{I}_{1-x}\text{Br}_x)_3$ layer blocks electrons and facilitates holes' collection.

Current density voltage (J - V) curves for the best devices, when Cu/Au and Cu/ $\text{MAPb}(\text{I}_{1-x}\text{Br}_x)_3$ /Au are used as back contacts, in forward to reverse bias voltage directions are shown in Figure 3A. In the perovskite back contact, J - V measurements were also conducted in forward to reverse and reverse to forward bias voltage directions to see any changes in the performance as changes have been seen in perovskite thin-film solar cells where perovskite is used as an absorber layer.⁴⁰ We did not find any appreciable differences in these measurements as shown in Figure S2.⁴¹ The J - V parameters for each type of contact are shown in Table 1. From Table 1 and Figure 3A, the performance improvement of devices in novel back contact is very clear

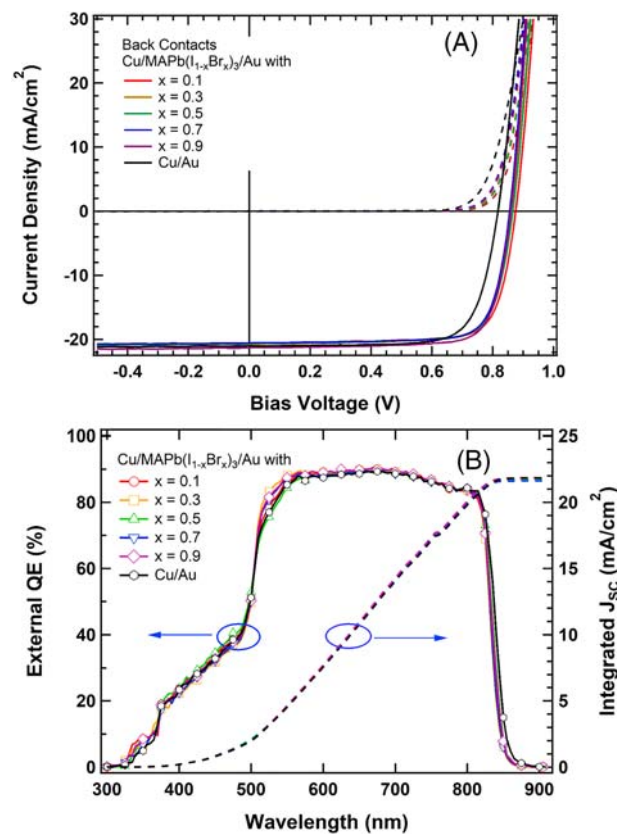


FIGURE 3 A, Current density-voltage characteristics of CdTe solar cells at Cu/Au and Cu/ $\text{MAPb}(\text{I}_{1-x}\text{Br}_x)_3$ /Au back contacts for different values of x measured at AM1.5G solar illumination; and B, external quantum efficiency (EQE) of solar cells for the Cu/Au and Cu/ $\text{MAPb}(\text{I}_{1-x}\text{Br}_x)_3$ /Au back contacts along with their integrated J_{sc} [Colour figure can be viewed at wileyonlinelibrary.com]

with $\sim 7\%$ increase in V_{OC} and $\sim 10\%$ increase in overall photo-conversion efficiency. In these devices, more than 3% improvement in FF is achieved with respect to the standard back contact as shown in Table 1. However, more than 7% improvement in FF has also been achieved with the application of perovskite film with the highest FF of 81%. The increase in FF was seen repeatedly when the Br concentration was increased from 0.1 to 0.9. Short circuit current densities, similar in all back contacts but lower in comparison to normal CdTe solar cells,^{8,11} are affected by slightly thicker CdS layer as is clear from the

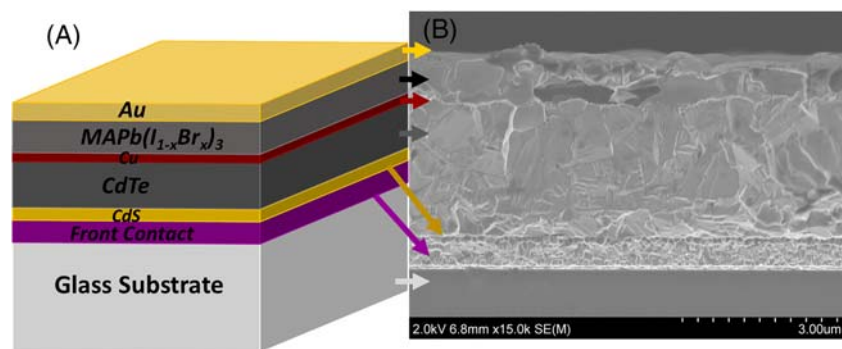


FIGURE 2 A, Device structure of a CdS/CdTe complete solar cell when $\text{MAPb}(\text{I}_{1-x}\text{Br}_x)_3$ is used as an interface layer. B, Cross-sectional imaging obtained by using scanning electron microscopy. [Colour figure can be viewed at wileyonlinelibrary.com]

TABLE 1 Best performance parameters of the solar cells with J-V curves in Figure 3A when using Cu/Au and Cu/MAPb(I_{1-x}Br_x)₃/Au back contacts measured at $t = 0$ h

Back contacts						
Cu/MAPb(I _{1-x} Br _x) ₃ /Au	V _{OC} (V)	J _{SC} (mA/cm ²)	FF (%)	η (%)	R _S (Ω cm ²)	R _{sh} (Ω cm ²)
x = 0.1	0.875	20.6	77.3	13.9	3.3	2604
x = 0.3	0.862	20.7	77.5	13.8	2.1	2370
x = 0.5	0.866	20.7	77.8	13.9	2.1	2209
x = 0.7	0.856	20.6	77.9	13.7	3.1	3216
x = 0.9	0.859	21.3	77.8	14.2	3.2	2261
Cu/Au	0.817	21.0	75.3	12.9	2.5	3807

collection loss in the wavelength range from 400 to 512 nm shown in EQE data in Figure 3B. The improvement in J_{SC} is seen for $x = 0.9$ where bandgap of perovskite is 2.22 eV. So, probability of absorption of photons of energy ≥ 2.22 eV and contributing photocurrent is not zero but definitely small. The improvement in photocurrent is mainly due to the reduction in recombination loss at the back contact interface with the addition of perovskite layer. Figure 3B shows EQE with back contacts of Cu/Au and Cu/MAPb(I_{1-x}Br_x)₃/Au where the variation in J_{SC} is very small with similar carrier collection in all regions of the spectrum. The integrated J_{SC} values obtained from the EQE spectra vary very little and agree very well with their counterparts measured from the J-V measurements as shown in Figure 3.

If we compare this work with one of the best CdS/CdTe solar cells of similar device structure (except perovskite interface layer),⁹ we find that our average V_{OC} is 19 mV higher, our average FF is 2.7% higher, but average J_{SC} is 4.28 mA/cm² smaller. Similarly, comparing this work with another highly efficient CdTe solar cell of slightly different device structure¹⁴ (CTO/ZTO/CdS/CdTe), it is found that the average V_{OC} in the present work is also 19 mV higher, average FF in this work is 2.3% higher, but average J_{SC} is 5.08 mA/cm² smaller. If J_{SC} is increased to 25 mA/cm², the efficiency in the present work can be increased to 16.9%, higher than given in Britt and Ferekides⁹ ($\eta = 15.8\%$) and Wu¹⁴ ($\eta = 16.5\%$).

The thickness of MAPb(I_{1-x}Br_x)₃ is yet to optimize, but the thickness as seen in Figure 2 (~750 nm) provides the best performance of the solar cells. This thickness is achieved in one-step deposition from the solution concentration discussed in Section 2. High-quality uniform film fabrication of MAPb(I_{1-x}Br_x)₃ using one-step deposition process depends on the surface morphology of CdCl₂-treated CdTe. If the surface morphology of CdTe is rough, MAPb(I_{1-x}Br_x)₃ does not easily wet CdTe surface and ends up with slightly nonuniform (variable thickness) MAPb(I_{1-x}Br_x)₃ films formation and, finally, nonuniform performance variation. The nonuniform film formation is usually found when the Br concentration is low. When Br concentration is increased in the precursor solution, MAI etching effect is reduced, and at higher Br concentration, Cd/Te ratio in CdTe remains fixed. When we add perovskite layer on top of CdTe surface, Cd strongly bonded with Te does not help to increase the grain size of perovskite because this is not a free Cd. The already occupied Cd does not work as a nucleation source for perovskite film to grow. So, there will not be an

enhancement of grain size of perovskite films deposited onto the CdTe surface when Br concentration is increased. However, film uniformity has been increased when Br concentration is increased as shown in Figure S3. We found that the MAPb(I_{0.9}Br_{0.1})₃ film of thickness about half of given in Figure 2 yields comparatively higher series resistance and lower V_{OC} similar to the Cu/Au back contact as shown in Figure 4. Because the thin perovskite film is porous, Au might easily penetrate through it and reach CdTe surface. Similarly, thicker MAPb(I_{0.9}Br_{0.1})₃ films yield higher series resistance with poor FF of the solar cells even though V_{OC} was acceptable as shown in Figure 4. In this case, photogenerated holes have to travel longer resistive pathway, as the perovskite is intrinsic with low carrier concentration, to reach the back contact metals and reduce its performance. The SEM cross-sectional imaging for the thin and thick MAPb(I_{0.9}Br_{0.1})₃ are shown in Figure S4.

Along with the single-step deposition of MAPb(I_{1-x}Br_x)₃, two-step deposition was also used to finish the back contacts for CdTe solar cells. Detailed work for performance optimization in two step deposition method is still to be conducted, but our preliminary measurements show comparatively poor performance than the single-step

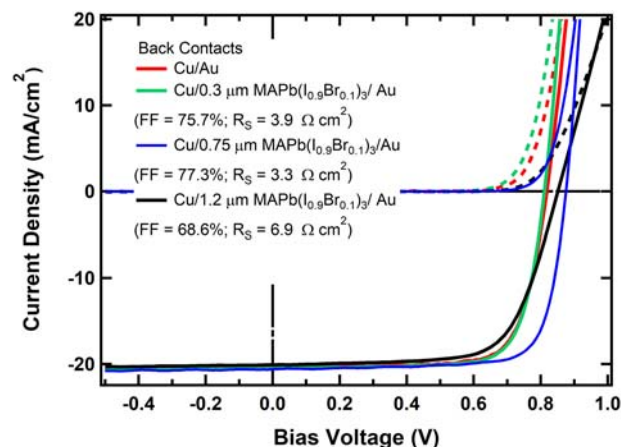


FIGURE 4 Current density-voltage characteristics of CdTe solar cells at Cu/Au and Cu/MAPb(I_{0.9}Br_{0.1})₃/Au back contacts measured at AM1.5G solar spectrum; variation of FF and series resistance with respect to perovskite film thickness is given in the figure [Colour figure can be viewed at wileyonlinelibrary.com]

method, but they are still promising for optimization as shown in Figure S5. The two-step deposition processes facilitate high-quality surface morphology of the film even though the device performance is poor. The poor performance may be due to the lack temperature optimization to the formation of perovskite.

Because the electron affinity of MAPbI₃ is ~4.1 eV^{42,43} and bandgap is ~1.55 eV⁴⁴ ($E_g = 1.6$ eV in present work), its work function is slightly smaller than the work function of Au¹² and generates barrier-free ohmic back contact with Au. However, as the work function of CdTe is higher (more negative) than the work function of MAPbI₃, barrier-free interface is not expected at CdTe/MAPbI₃ heterojunction. The bandgap of MAPbI₃ can be tuned in the range of ~1.6 to ~2.3 eV (see Figure S1 for transmission and bandgap calculation) by introducing Br to the formation of MAPb(I_{1-x}Br_x)₃.³³ For the formation of valence band maximum (VBM) in MAPbX₃, strong contribution of X p states with Pb s states is required, but for the formation of conduction band minimum (CBM), only a small contribution of X s orbital with Pb p orbital is sufficient. When part of the iodine (I) is substituted by bromine (Br), the Br 4p states tend to hybridize more strongly with Pb s states than with I 5p states and causes the downshift of VBM.⁴⁵ Therefore, when bandgap increases with the incorporation of Br, shift of valence band to higher negative energy is expected more than shift of conduction band to smaller energy. This process minimizes the valence band offset with the CdTe, creating very low barrier energy at CdTe/MAPb(I_{1-x}Br_x)₃ interface.⁴⁶⁻⁴⁸ In this case, work function of MAPb(I_{1-x}Br_x)₃ also shifts to the direction of negative energy, minimizing the work function difference between two semiconductors. The energy barrier generated at the back contact interface is therefore reduced as will be clear by the temperature-dependent J-V measurement (*vide infra*). Note that MAPb(I_{1-x}Br_x)₃ is used as a semiconductor interface layer rather than a back contact, and MAPb(I_{1-x}Br_x)₃ is an intrinsic semiconductor with very low carrier density, and CdTe is Cu-doped p-type semiconductor. When these two semiconductors are in contact, there is diffusion of electrons from MAPb(I_{1-x}Br_x)₃ to CdTe because electrons tend to move downhill. Because MAPb(I_{1-x}Br_x)₃ is intrinsic, number of electrons available for the diffusion to CdTe side is not very large, and because the Cu-doped CdTe surface has excessive holes as majority charge carriers, the depletion width so formed at the interface is very narrow. This also explains that the barrier generated at the Cu-doped CdTe/MAPbI₃ interface is smaller than the barrier at Cu-doped CdTe/Au interface.

Therefore, performance improvement in novel back contact is ascribed by the reduced back contact barrier and the potential for the electron-reflecting behavior at the CdTe/MAPb(I_{1-x}Br_x)₃ interface. To determine the barrier height at the back contact to the CdTe solar cell, temperature-dependent current-voltage (I-V) measurement method described by Niemegeers and Burgelman was used.⁴ For this, temperature dependence of the current when devices were placed into forward bias was measured. The concept of the measurement takes into the consideration of two opposing diodes connected in series. When the device is placed in forward bias, the front diode developed at CdS/CdTe interface is forward biased, but the back diode developed at back contact interface is reverse biased. The reverse-biased diode

limits the charge flow due to the back contact barrier, Φ_b , which can be the source of recombination loss and degrades V_{OC} and FF of the solar cells.

Figures S6 show the measured I-V curves for CdTe solar cells in the dark for Cu/Au and Cu/MAPb(I_{1-x}Br_x)₃/Au back contacts, respectively, at temperature from 180 K to 300 K. Qualitatively, significant lower back contact barrier height is observed for novel back contact with respect to the standard back contact. Note that the value of the current even at <2 V forward bias is greater than 10⁻⁴ A for Cu/MAPb(I_{1-x}Br_x)₃/Au at all temperatures, whereas the current for the Cu/Au contact is less than 10⁻⁴ A for temperatures of 220 K and below.

To develop a quantitative assessment of Φ_b , we consider two carrier transport mechanisms: thermionic emission (TE) model and drift-diffusion (DD) model given by following two equations.⁴

$$J \propto T^2 \exp\left(-\frac{e\Phi_b}{kT}\right), \quad (1)$$

$$J \propto T^{\frac{3}{2}} \exp\left(-\frac{e\Phi_b}{kT}\right). \quad (2)$$

These two equations were used to plot the experimental data and to find out back contact barrier height. Figure 5 shows plots of $\ln(J/T^2)$ and $\ln(J/T^{1/2})$ versus $1/KT$ for CdTe solar cells completed with Cu/Au and Cu/MAPb(I_{1-x}Br_x)₃/Au back contacts. The linear slope of the plots in the temperature from 180 K to 300 K is used to provide the measurement of Φ_b . Within each model, the barrier height for Cu/MAPb(I_{1-x}Br_x)₃/Au back contact is lower than that of Cu/Au back contact as shown in Figure 5. As per our hypothesis, we also found that as the Br concentration is increased from 0.1 to 0.9, the barrier height is decreased from 178 meV to 121 meV in thermionic emission model and 209 meV to 148 meV in drift-diffusion model as shown in Figure 5 and Table 2.

The concentration of additional Br in MAPb(I_{1-x}Br_x)₃ may be helpful in improving the device performance as can be seen some improvement in J_{SC} and FF. This improvement in performance may be due to the proper band alignment as is verified by the temperature-dependent study. The detailed analysis of this band alignment is provided as following. Using electron affinity of ~4.1 eV and bandgap of ~1.55 eV, the work function of MAPbI₃, considering it as an intrinsic semiconductor, is ~4.875 eV, smaller than the work function for Au.¹² As the Br concentration increases, bandgap widens and the work function slowly shifts downward but still maintains the ohmic contact with Au until 90% of the Br concentration. If we suppose only the shift in VBM and CBM is fixed, then for 90% of Br concentration, the bandgap of MAPb(I_{0.1}Br_{0.9})₃ is ~2.2 (Figure S1) and corresponding VBM is ~6.3 eV. However, the shift of CBM cannot be completely ruled out, and hence the valence band matching with CdTe is very well expected. Very low barrier height (~0.135 eV in average) obtained for 90% of Br concentration is the indication of ohmic contact and valence band matching of two semiconductors. The very low

FIGURE 5 Plots for evaluating ϕ_b associated with Cu/Au and MaPb($1-x$ Br $_x$) $_3$ /Au back contacts to CdTe solar cells, according to thermionic emission transport (A, C, E, G) and drift-diffusion (B, D, F, H) models. The red lines indicate the nominally linear fitted regions [Colour figure can be viewed at wileyonlinelibrary.com]

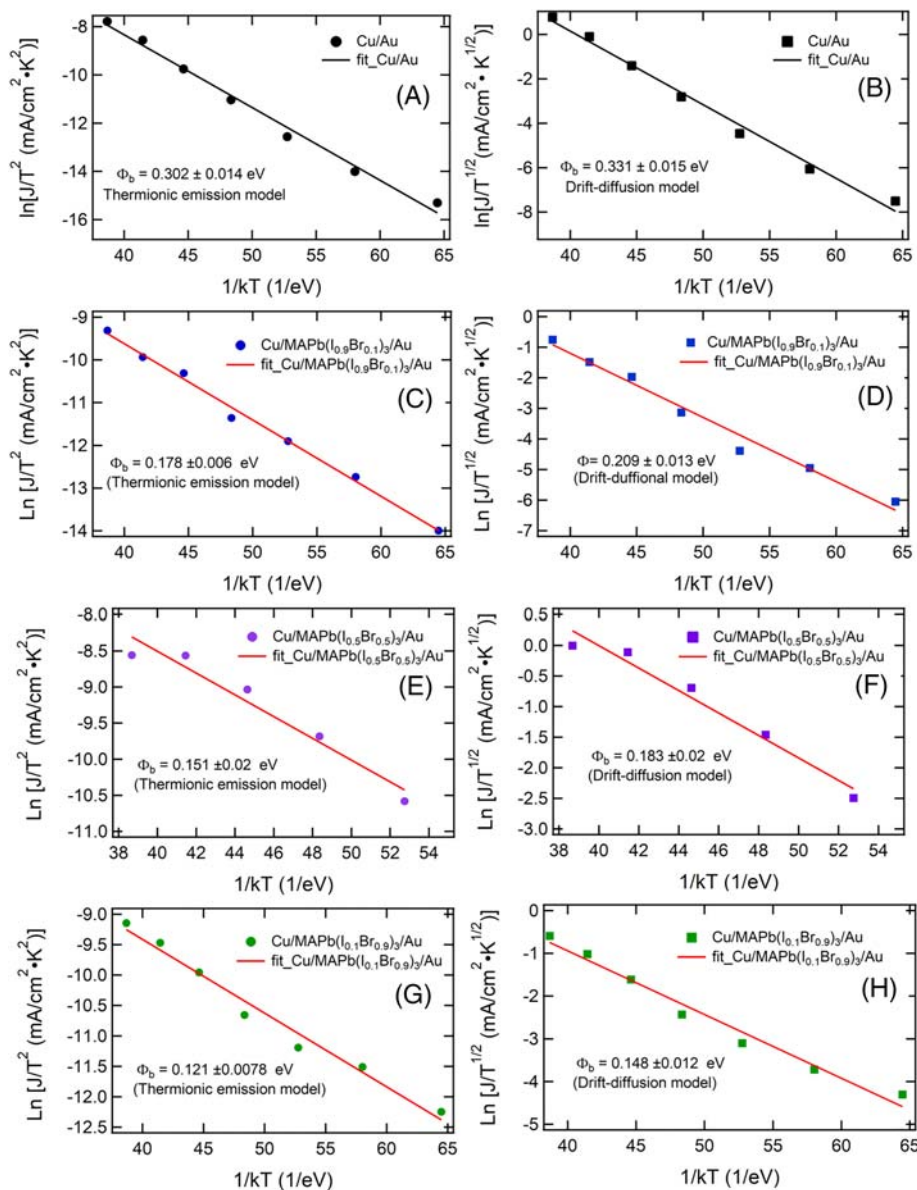


TABLE 2 Barrier height for CdTe solar cells when using Cu/Au and MAPb($1-x$ Br $_x$) $_3$ /Au back contacts

Model	Cu/Au	Cu/MAPb($1_{0.9}$ Br $_{0.1}$) $_3$ /Au	Cu/MAPb($1_{0.5}$ Br $_{0.5}$) $_3$ /Au	Cu/MAPb($1_{0.1}$ Br $_{0.9}$) $_3$ /Au
TE	0.302 ± 0.014	0.178 ± 0.006	0.151 ± 0.02	0.121 ± 0.007
DD	0.331 ± 0.015	0.209 ± 0.013	0.183 ± 0.019	0.148 ± 0.012
Avg.	0.317 ± 0.014	0.183 ± 0.009	0.167 ± 0.021	0.135 ± 0.009

Abbreviations: DD, drift-diffusion; TE, thermionic emission.

barrier height can also be understood by the repeated increase of FF with the increase of Br concentration from 0.1 to 0.9. The FF of 81% has also been reached for Br = 0.9 (Figure S7). This improvement is related to the valence band matching at CdTe/ZnTe interface.^{16,49} In the case of ZnTe as an interface layer to CdTe, the ZnTe must be highly Cu-doped to increase p-type (10^{18} – 10^{19} cm⁻³) conductivity to facilitate low-resistance tunneling to back contact metal.¹⁶ Without Cu doping, ZnTe generates large work function difference with back contact metals and creates barriers to photogenerated holes to reach

the back contact metals. For MAPb($1-x$ Br $_x$) $_3$, Cu doping is not necessary to create low-barrier interface with back contact metal. When the Br = 1, the bandgap is 2.31 eV, and hence the top of the valence band of MAPbBr $_3$ (~6.41 eV if only VBM shifts downward keeping CBM fixed) exceeds the top of the valence band of CdTe. This creates type-I heterojunction between CdTe/MAPbBr $_3$ interface, not favorable for high-performance solar cells. The performance of CdTe solar cells is decreased when MAPbBr $_3$ is used as an interface layer as shown in Figure S8. When using MAPbBr $_3$, V_{OC} was not very small

(max. of 0.849 V), but FF was very severely affected with a maximum of 74%, and high series resistance of $6 \Omega \text{ cm}^2$ was obtained.

Recently, Waththage et al. demonstrated that simply etching of CdTe surface by MAI produces elemental Te as confirmed by XRD and Raman spectroscopy measurements.⁵⁰ The authors, in their detailed analysis, concluded that the Te reach surface minimizes the Schottky barrier and found improvement in V_{OC} and FF of the solar cells. Because MAI is more reactive than MABr, it is possible that the Te layer thickness changes with Br concentration. This could lead to a thicker Te layer for lower Br. The 0.1 Br could have a “thick” Te layer with the perovskite on top, whereas the 0.9 Br could have no or negligible Te with perovskite on top. One experiment was conducted to check the effect of MAI etching on CdTe surface for $\text{MAPb}(\text{I}_{0.1}\text{Br}_{0.9})_3$ as an interface layer. To accomplish this, CdTe surface was etched with MAI solution before making $\text{Cu}/\text{MAPb}(\text{I}_{0.1}\text{Br}_{0.9})_3/\text{Au}$ back contacts. For the comparison, same back contacts were also applied in other samples without first etching with MAI. Current density voltage measurement was conducted in both samples, and their J-V curves are provided in Figure S9. It is found that the performance of the solar cells with MAI etching is better than without etching. This explains why the V_{OC} is lower for 0.9 Br than for 0.1 Br as shown in Figure 3 and Table 1. To check the Te-rich surface on CdTe, MAPbI_3 film was first prepared, washed with DMF, and SEM imaging and Raman spectroscopy measurement were conducted. The SEM imaging confirms Te-rich surface (Figure 6A,B), and Raman spectrum shows very intense Te peaks on perovskite-treated film, whereas these peaks were missing on untreated sample as shown in Figure 6. We see two active Raman phonon modes. The most intense Raman peak of Te is located at 122.5 cm^{-1} and is related to the A_1 mode in which each atom moves in the basal plane, and the other mode located at 141 cm^{-1} is E^2 mode and is related to asymmetric stretching mainly along the c-axis.⁵¹ These peaks were seen only on treated

sample, but untreated sample has no peak at all as shown in Figure 6C.

Finally, part of the stability test, not rigorous in nature, was completed for the devices having perovskite interface layer. To accomplish this test, a solar cell was stored in an inert atmosphere (N_2 environment) and its J-V measurement was again completed on the 7th and 27th days. The efficiency of the solar cell was improved by $\sim 7\%$. As shown in Figure S10 and Table S2, V_{OC} and FF of the device were improved. As stated in Section 2, perovskite thin film was fabricated in an ambient environment. Stability test has not been conducted yet by storing the devices in air. The cause of this improvement and more stability tests are subjects of our future work.

4 | CONCLUSIONS

We have demonstrated that organo-metallic halide perovskite, a successful absorber layer in thin-film solar cells, can be a promising hole transport material in CdTe thin-film solar cells. Perovskite $\text{MAPb}(\text{I}_{1-x}\text{Br}_x)_3$ thin films are fabricated by solution-based cost-effective approach at low temperature. Our results indicate that application of perovskite as an interface layer in CdTe solar cells enhances the performance and by reducing Schottky barrier generated at the CdTe/metal interface. Our preliminary results showed $\sim 10\%$ increase in photoconversion efficiency with the introduction of perovskite with respect to standard Cu/Au back contacts. The stabilities of CdTe and perovskite solar cells for standard back contacts are not new to scientific communities. The stability of our solar cells in perovskite back contact is determined by the stability of perovskite. Our work on CdTe solar cells with perovskite proves the very important concept regarding the back contact of CdTe solar cells. From this work, we conclude that back contact management in CdTe solar cells is crucial to gain full achievement. Our experiment also opened a new

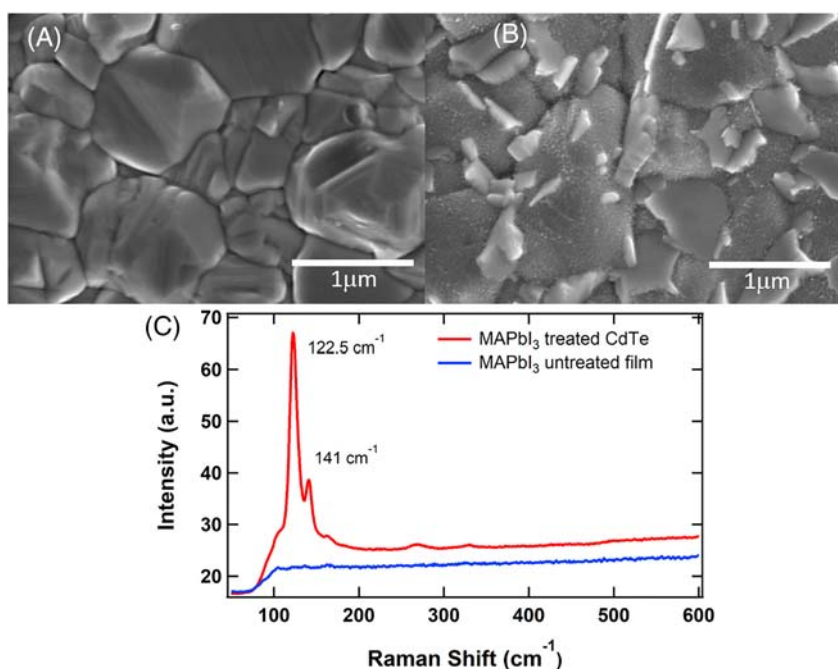


FIGURE 6 A, Scanning electron microscopy (SEM) image of CdTe before MAPbI_3 treatment, B, SEM image of CdTe when a thin layer of MAPbI_3 deposition was completed and cleaned by dimethylformamide (DMF), and C, Raman spectra of (A) and (B) [Colour figure can be viewed at wileyonlinelibrary.com]

avenue of research for perovskite solar cells, that is, CdTe thin film can be used as an electron transport layer in perovskite solar cells.

ACKNOWLEDGEMENT

The authors gratefully acknowledge financial support provided by the National Science Foundation's Sustainable Energy pathways program (CHE-1230246) and the U.S. Air Force Research Laboratory (FA9453-11-C-0253).

ORCID

Khagendra P. Bhandari  <https://orcid.org/0000-0002-4386-6301>

Zhaoning Song  <https://orcid.org/0000-0002-6677-0994>

REFERENCES

- Adachi S. *Optical Constants of Crystalline and Amorphous Semiconductors: Numerical Data and Graphical Information*. Springer Science & Business Media; 1999.
- Green MA, Emery K, Hishikawa Y, Warta W, Dunlop ED. Solar cell efficiency tables (version 48). *Prog Photovolt Res Appl*. 2016;24(7):905-913.
- Shockley W, Queisser HJ. Detailed balance limit of efficiency of p-n junction solar cells. *J Appl Phys*. 1961;32(3):510-519.
- Niemegeers A, Burgelman M. Effects of the Au/CdTe back contact on IV and CV characteristics of Au/CdTe/CdS/TCO solar cells. *J Appl Phys*. 1997;81(6):2881-2886.
- Yang J-H, Yin W-J, Park J-S, et al. Enhanced p-type dopability of P and As in CdTe using non-equilibrium thermal processing. *J Appl Phys*. 2015;118(2):25102-1-25102-6.
- Demtsu S, Albin D, Sites J. Role of copper in the performance of CdS/CdTe solar cells, Photovoltaic Energy Conversion, *Conference Record of the 2006 IEEE 4th World Conference on, IEEE*: 2006:523-526.
- Gupta A, Compaan AD. All-sputtered 14% CdS/ CdTe thin-film solar cell with ZnO:Al transparent conducting oxide. *Appl Phys Lett*. 2004;85(4):684-686.
- Paudel NR, Yan Y. Fabrication and characterization of high-efficiency CdTe-based thin-film solar cells on commercial SnO₂: F-coated soda-lime glass substrates. *Thin Solid Films*. 2013;549:30-35.
- Britt J, Ferekides C. Thin-film CdS/CdTe solar cell with 15.8% efficiency. *Appl Phys Lett*. 1993;62(22):2851-2852.
- Gessert T, Sheldon P, Li X, Dunlavy D, Niles D, Sasala R, Albright S, Zadler B. Studies of ZnTe back contacts to CdS/CdTe solar cells, *Photovoltaic Specialists Conference, 1997.*, Conference Record of the Twenty-Sixth IEEE, IEEE: 1997:419-422.
- Mahabaduge H, Rance W, Burst J, et al. High-efficiency, flexible CdTe solar cells on ultra-thin glass substrates. *Appl Phys Lett*. 2015;106(13):1-4. 133501.
- Bhandari KP, Koirala P, Paudel NR, et al. Iron pyrite nanocrystal film serves as a copper-free back contact for polycrystalline CdTe thin film solar cells. *Solar Energy Mater Solar Cells*. 2015;140:108-114.
- Bhandari KP, Tan X, Zereshki P, et al. Thin film iron pyrite deposited by hybrid sputtering/co-evaporation as a hole transport layer for sputtered CdS/CdTe solar cells. *Solar Energy Mater Solar Cells*. 2017;163:277-284.
- Wu X. High-efficiency polycrystalline CdTe thin-film solar cells. *Solar Energy*. 2004;77(6):803-814.
- Green MA, Hishikawa Y, Dunlop ED, Levi DH, Hohl-Ebinger J, Ho-Baillie AW. Solar cell efficiency tables (version 51). *Prog Photovolt Res Appl*. 2018;26(1):3-12.
- Rioux D, Niles DW, Höchst H. ZnTe: a potential interlayer to form low resistance back contacts in CdS/CdTe solar cells. *J Appl Phys*. 1993;73(12):8381-8385.
- Kolesnyk M, Opanasyuk A, Tyrkusova N, Danilchenko S. ZnTe/CdTe thin-film heterojunctions. *J Nano Electron Phys*. 2009;1(2):8-17.
- Geisthardt RM, Topić M, Sites JR. Status and potential of CdTe solar-cell efficiency. *IEEE J Photovolt*. 2015;5(4):1217-1221.
- Zhao Y, Boccard M, Liu S, et al. Monocrystalline CdTe solar cells with open-circuit voltage over 1 V and efficiency of 17%. *Nat Energy*. 2016;1(6):16067.
- Song Z, Waththage SC, Phillips AB, Heben MJ. Pathways toward high-performance perovskite solar cells: review of recent advances in organo-metal halide perovskites for photovoltaic applications. *J Photon Energy*. 2016;6(2):22001-22001.
- Snaith HJ. Perovskites: the emergence of a new era for low-cost, high-efficiency solar cells. *J Phys Chem Lett*. 2013;4(21):3623-3630.
- Gao P, Grätzel M, Nazeeruddin MK. Organohalide lead perovskites for photovoltaic applications. *Energy Environ Sci*. 2014;7(8):2448-2463.
- Stranks SD, Snaith HJ. Metal-halide perovskites for photovoltaic and light-emitting devices. *Nat Nanotechnol*. 2015;10(5):391-402.
- Zhou H, Chen Q, Li G, et al. Interface engineering of highly efficient perovskite solar cells. *Science*. 2014;345(6196):542-546.
- Nie W, Tsai H, Asadpour R, et al. High-efficiency solution-processed perovskite solar cells with millimeter-scale grains. *Science*. 2015;347(6221):522-525.
- Seo J, Noh JH, Seok SI. Rational strategies for efficient perovskite solar cells. *Acc Chem Res*. 2016;49(3):562-572.
- Gessert T, Mason A, Sheldon P, Swartzlander A, Niles D, Coutts T. Development of Cu-doped ZnTe as a back-contact interface layer for thin-film CdS/CdTe solar cells. *J Vac Sci Technol A*. 1996;14(3):806-812.
- Fan Y, Han J, He L, et al. Electrical transport characterizations of nitrogen doped ZnSe and ZnTe films. *J Electr Mater*. 1994;23(3):245-249.
- Bhandari KP, Waththage SC, Song Z, Phillips A, Heben MJ, Ellingson RJ. Applications of hybrid organic-inorganic metal halide perovskite thin film as a hole transport layer in CdTe thin film solar cells, *IEEE 44th Photovoltaic Specialist Conference (PVSC)*, 25-30 June 2017. 2017:748-751.
- Oku T. *Crystal structures of CH₃NH₃PbI₃ and related perovskite compounds used for solar cells*. *Solar Cells-New Approaches and Reviews*. InTech; 2015.
- Ahn N, Son D-Y, Jang I-H, Kang SM, Choi M, Park N-G. Highly reproducible perovskite solar cells with average efficiency of 18.3% and best efficiency of 19.7% fabricated via Lewis base adduct of lead (II) iodide. *J Am Chem Soc*. 2015;137(27):8696-8699.
- McCandless BE, Birkmire RW, Buchanan WA. Vapor transport deposition of cadmium telluride films, *Photovoltaic Specialists Conference, 2002*. Conference Record of the Twenty-Ninth IEEE, IEEE: 2002:547-550.
- Noh JH, Im SH, Heo JH, Mandal TN, Seok SI. Chemical management for colorful, efficient, and stable inorganic-organic hybrid nanostructured solar cells. *Nano Lett*. 2013;13(4):1764-1769.
- Sadhanala A, Deschler F, Thomas TH, et al. Preparation of single-phase films of CH₃NH₃Pb(I_{1-x}Br_x)₃ with sharp optical band edges. *J Phys Chem Lett*. 2014;5(15):2501-2505.
- Mosconi E, Amat A, Nazeeruddin MK, Grätzel M, De Angelis F. First-principles modeling of mixed halide organometal perovskites for photovoltaic applications. *J Phys Chem C*. 2013;117(27):13902-13913.
- Atourki L, Vega E, Mari B, et al. Role of the chemical substitution on the structural and luminescence properties of the mixed halide perovskite thin MAPb_{3-x}Br_x (0 ≤ x ≤ 1) films. *Appl Surf Sci*. 2016;371:112-117.
- Tu Y, Wu J, Lan Z, et al. Modulated CH₃NH₃PbI_{3-x}Br_x film for efficient perovskite solar cells exceeding 18%. *Sci Rep*. 2017;7(1):44603.
- Potlog T, Spalatu N, Maticiu N, et al. Structural reproducibility of CdTe thin films deposited on different substrates by close space sublimation method. *Phys Stat Solid (A)*. 2012;209(2):272-276.

39. Oku T. Crystal structures of $\text{CH}_3\text{NH}_3\text{PbI}_3$ and related perovskite compounds used for solar cells. *Solar Cells-New Approach Rev.* 2015;1: 77–101.
40. Unger EL, Hoke ET, Bailie CD, et al. Hysteresis and transient behavior in current-voltage measurements of hybrid-perovskite absorber solar cells. *Energ Environ Sci.* 2014;7(11):3690-3698.
41. Bhandari KP, Waththage SC, Song Z, Phillips AJ, Heben MJ, Ellingson RJ. *Applications of hybrid organic-inorganic metal halide perovskite thin film as a hole transport layer in CdTe thin film solar cells.* Photovoltaic Specialist Conference Washington D. C. Washington D. C: IEEE PVSC 44; 2017:4.
42. Schulz P, Edri E, Kirmayer S, Hodes G, Cahen D, Kahn A. Interface energetics in organo-metal halide perovskite-based photovoltaic cells. *Energ Environ Sci.* 2014;7(4):1377-1381.
43. Frost JM, Butler KT, Brivio F, Hendon CH, van Schilfgaarde M, Walsh A. Atomistic origins of high-performance in hybrid halide perovskite solar cells. *Nano Lett.* 2014;14(5):2584-2590.
44. Giorgi G, Fujisawa J-I, Segawa H, Yamashita K. Small photocarrier effective masses featuring ambipolar transport in methylammonium lead iodide perovskite: a density functional analysis. *J Phys Chem Lett.* 2013;4(24):4213-4216.
45. Jong U-G, Yu C-J, Ri J-S, Kim N-H, Ri G-C. Influence of halide composition on the structural, electronic, and optical properties of mixed $\text{CH}_3\text{NH}_3\text{Pb}(\text{I}_{1-x}\text{Br}_x)_3$ perovskites calculated using the virtual crystal approximation method. *Phys Rev B.* 2016;94(12):125139.
46. Zhou X, Ye W, Li X, et al. Band alignment of $\text{MAPb}(\text{I}_{1-x}\text{Br}_x)_3$ thinfilms by vacuum deposition. *Appl Phys Lett.* 2016;109(23): 233906-1–233906-4.
47. Liga SM. Components-bandgap relationships in hybrid organic-inorganic perovskites. 2017.
48. Park B-W, Philippe B, Jain S, et al. Chemical engineering of methylammonium lead iodide/bromide perovskites: tuning of optoelectronic properties and photovoltaic performance. *J Matter Chem A.* 2015;3:21760-21771.
49. Fahrenbruch AL. Ohmic contacts and doping of CdTe. *Solar Cells.* 1987;21(1–4):399-412.
50. Waththage SC, Phillips AB, Liyanage GK, et al. Selective Cd removal from CdTe for high-efficiency Te back-contact formation. *IEEE J Photovolt.* 2018;8(4):1125-1131.
51. Du Y, Qiu G, Wang Y, et al. One-dimensional van der Waals material tellurium: Raman spectroscopy under strain and magneto-transport. *Nano Lett.* 2017;17(6):3965-3973.

SUPPORTING INFORMATION

Additional supporting information may be found online in the Supporting Information section at the end of this article.

How to cite this article: Bhandari KP, Alfadhili FK, Bastola E, et al. Very high V_{OC} and FF of CdTe thin-film solar cells with the applications of organo-metallic halide perovskite thin film as a hole transport layer. *Prog Photovolt Res Appl.* 2020;1–10. <https://doi.org/10.1002/ppp.3309>